Analysis of the resonance phenomenon in unmatched power cables with the resonance surface response

Tamiris Bade, James Roudet, Jean-Michel Guichon, Patrick Kuo-Peng, Carlos A.F. Sartori

Analysis of the Resonance Phenomenon in Unmatched Power Cables: the Resonance Surface Response

Tamiris G. Bade[a,*], James Roudet[a], Jean-Michel Guichon[a], Patrick Kuo-Peng[b], Carlos A.F. Sartori[c]

[a] *Univ. Grenoble Alpes, CNRS, Grenoble INP, G2Elab, 21 av des martyrs 38000 Grenoble, France*
[b] *Federal University of Santa Catarina, GRUCAD, campus Trindade, Florianópolis 88040-970, Brazil*
[c] *Escola Politécnica da Universidade de São Paulo (PEA/EPUSP), São Paulo 05508-010, SP, Brazil, with Instituto de Pesquisas Energéticas e Nucleares (IPEN/CNEN-SP),São Paulo 05508-900, SP, Brazil*

Abstract

The resonance phenomenon has become more common in the recent years with the increase of the power converter applications in power systems. Resonance can cause serious damages, and must be taken into account on the design phase of power systems whenever possible. The resonance surface response is a new method of analysis that allows the evaluation of the resonance-due voltage and/or current amplification in transmission lines, along with the resonance frequency and the position along the line where the amplification takes place. The surfaces can be calculated for any linear system under the risk of the resonance phenomenon in a transmission line or long cable, independently of its number of conductors. This analysis can be useful to determine the adequate choice of the critical insulation voltage of a cable, to design robust output filters for power converters connected to long cables, to mitigate EMI phenomenon such as cross-talk, etc... Here the theory and allowing the resonance surface response computation is presented. Two examples of surfaces are given: a three-dimensional surface to describe the resonance in a two-conductor cable and a seven-dimensional surface for a three-conductor cable; the later is analyzed with

*Corresponding author
Email address: tamiris.grossl-bade@g2elab.grenoble-inp.fr (Carlos A.F. Sartori)

an optimization algorithm. The dependency of the resonance on the cable length and the difficulties that arise from the analysis of higher dimensional surfaces are discussed.
Keywords: Power Cable, Resonance, Switching harmonics, Power converters, EMC

1. Introduction

In recent years the insertion of power converters on power systems is increasing considerably. At the same time the filters responsible for attenuating the switching harmonics generated by the converters tend to be reduced, or even absent, whenever possible. These tendencies contribute to electromagnetic interference (EMI) problems on power systems by increasing the conducted emissions in the system [1].

These conducted emission may be amplified by the resonance phenomenon if they circulate through a long cable. Some examples of applications where the switching harmonics may cause damage to the installation are: the connections between offshore power plants and the onshore substations [2, 3]; in electric transportation applications such as trains (catenary lines) [4], electric automobiles [5] or more electric aircraft [6]; and on long power cables connecting AC motors to its drives [7, 8, 9, 10, 11].

With the advent of wide-band gap semiconductors these dangerous resonance-due overvoltages and overcurrents tend to appear in shorter cables, because the commutation times will be faster and introduce harmonics up to higher frequencies. Therefore, an effective design method able to increase the robustness of a system facing resonance tend only to become more relevant.

The difficulties of an accurate model of the resonance arise from frequency-dependent behavior of the power cables used in these applications [12]. With frequency-dependent per-unit-length (p.u.l.) parameters comes a frequency-dependent propagation speed [13], and to determine the resonance frequency of such cables a numerical solution is indispensable [14, 15]. The paper [14] gives

an efficient method to calculate the resonance frequency for transmission lines connected to resistive loads, however, it cannot be applied to reactive loads. Knowledge on the resonance frequency is useful in many of the applications aforementioned, notably for resonance damping methods based on notch filters [3], which are likely to be reactive.

This paper describes an innovative analysis and representation method: the "resonance surface response". It describes the behavior of the resonance phenomenon in a given multiconductor transmission line in function of the impedances connected to its terminals. It gives a more general description of the resonance behavior than the present literature because it allows the description of the resonance phenomenon, giving its frequency, position and amplification, for a generic linear system with any number of conductors in the line.

Of course, in all the resonant cables aforecited the perturbations are originated by power converters, therefore their linear equivalent model is necessary if they are to be included on the system simulations. For an EMI study, such as the one proposed in this paper, a high frequency linear model as described in [16, 17] is sufficient.

The analysis proposed here is performed for the medium frequency band, from hundreds of kHz to tens of MHz, and can be particularly useful in the design of robust EMC filters. However, the method can be easily adapted to other frequency band, the only limitation of the model arising from the validity of the equivalent linear model chosen for the power converters. Indeed, there are some cases of dangerous resonance amplification in low frequencies such as large-scale distributed power plants [18, 19] and offshore power plants [20], to which a transfer function model of the converter is more convenient.

In this paper the analysis of asymmetric multiconductor systems with the resonance surface response is described in firsthand, what leads to the scrutiny of a higher dimensional surface with an optimization algorithm. Also, the theoretical aspects of the resonance surface response are detailed and different analysis deriving from this approach are exploited. For a direct example of their applicability please refer to [21] where the resonance surface response was first

introduced by the authors, but know that this previous paper is limited to the analysis of three-conductor balanced systems, with the surfaces represented on no more than three dimensions.

The resonance surface response method in its most generic form is described in section 2. A first example of a two-conductor transmission line leading to three-dimensional resonance surface responses is shown in section 3, and an example with a three-conductor transmission line giving seven-dimension surfaces is detailed in section 4.

2. The resonance in transmission lines

The resonance phenomenon may occur in transmission lines (TL) as in many other physical systems: if the line impedances are not matched, the voltage and current waves traveling through the line are reflected at its terminals and at specific frequencies their superposition leads to an amplification of the excitation wave.

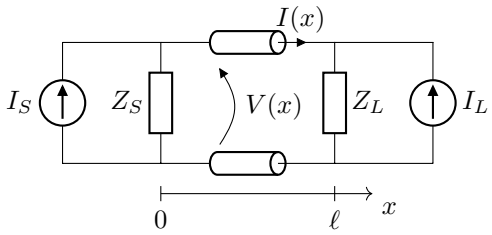

Figure 1: Schematics of a generic two-conductor cable system, Norton equivalents at the terminals

A generic two-conductor system is represented in Fig. 1. Its reflection coefficients are given by equations (1) and (2), and the condition of matched impedances is in (3). In these equations, Z_c is the characteristic impedance of the line.

$$\Gamma_L = \frac{Z_L - Z_c}{Z_L + Z_c} \tag{1}$$

$$\Gamma_S = \frac{Z_S - Z_c}{Z_S + Z_c} \tag{2}$$

$$Z_L = Z_S = Z_c \tag{3}$$

In power electronics applications the cables and devices are unlikely to have matched impedances, and medium frequency harmonics are present due to the switched current and voltage in the converter. If some of these harmonics match the natural frequencies of the cable, they might be amplified by the resonance phenomenon.

The natural frequencies of a TL can be found by minimizing its input impedance (4). Finding these minima analytically is complicated: the variables Z_S, Z_L, Z_c and γ are frequency dependent, what makes the derivative of (4) in relation to the frequency too cumbersome.

$$Z(0) = Z_S \,//\, Z_c \frac{Z_L + Z_c \tanh(\ell\gamma)}{Z_c + Z_L \tanh(\ell\gamma)} \tag{4}$$

More specifically, the variations of γ with the frequency gives a frequency dependent propagation speed v, what demands a numerical solution for the resonance frequency even if the other variables were real constants, as shown in [14]. The aforecited paper gives a numerical method to determine the resonance frequency for $Z_S \to \infty$ and Z_L a resistive load, but not for a generic system.

The resonance behavior of a system with long cables will be numerically represented in this paper, and the simulations used for the results presented here are based on a frequency-domain simulator described and experimentally validated in [12].

The frequency-domain simulator is based on the numerical solution for $V(x)$ and $I(x)$ of equations (5) to (11) for each value of a discrete frequency vector. The equations model a system containing a $n+1$-conductor cable as shown in Fig. 2 when connected to generic multiport equivalent models are [22]:

$$\begin{bmatrix} \mathbf{V}(x) \\ \mathbf{I}(x) \end{bmatrix} = \begin{bmatrix} \mathbf{\Phi}_1(x) & \mathbf{\Phi}_2(x) \\ \mathbf{\Phi}_3(x) & \mathbf{\Phi}_4(x) \end{bmatrix} \begin{bmatrix} \mathbf{V}(0) \\ \mathbf{I}(0) \end{bmatrix} \tag{5}$$

$$\mathbf{\Phi}_1(x) = \mathbf{Z}_c \cosh(x\sqrt{\mathbf{YZ}})\mathbf{Y_c} \tag{6}$$

$$\mathbf{\Phi}_2(x) = -\mathbf{Z}_c \sinh(x\sqrt{\mathbf{YZ}}) \tag{7}$$

$$\mathbf{\Phi}_3(x) = -\sinh(x\sqrt{\mathbf{YZ}})\mathbf{Y_c} \tag{8}$$

$$\mathbf{\Phi}_4(x) = \cosh(x\sqrt{\mathbf{YZ}}) \tag{9}$$

$$\mathbf{I}(0) = \mathbf{I_S} - \mathbf{Y}_S\mathbf{V}(0) \tag{10}$$

$$-\mathbf{I}(\ell) = \mathbf{I_L} - \mathbf{Y}_L\mathbf{V}(\ell) \tag{11}$$

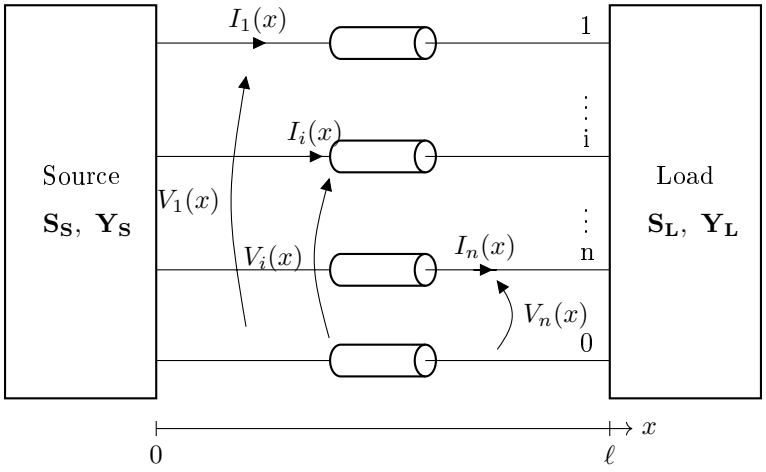

Figure 2: Generic system with multiconductor cable, devices or network connected to the cable terminals represented by Thévénin/Norton $n+1$-port equivalent circuits

In equations (5) to (9), x is the space axis parallel o the line, ℓ is the cable length, $\mathbf{I}$ and $\mathbf{V}$ are vectors of size n containing respectively the currents of each active conductor and the voltages relative to the reference conductor; $\mathbf{Z}_c = \mathbf{Y}^{-1}\sqrt{\mathbf{YZ}}$ is the characteristic impedance matrix,$\mathbf{Y}_c = \mathbf{Z}_c^{-1}$ is the characteristic admittance matrix and $\sqrt{\mathbf{YZ}}$ is the non-diagonalized propagation matrix. Matrices $\mathbf{Z} = \mathbf{R} + j\omega\mathbf{L}$ and $\mathbf{Y} = \mathbf{G} + j\omega\mathbf{C}$ are the p.u.l. impedance and admittance matrices, respectively. The definition of the p.u.l. resistance $\mathbf{R}$, inductance $\mathbf{L}$, conductance $\mathbf{G}$ and capacitance $\mathbf{C}$ matrices can be found in [22]; j is the imaginary unity and ω is the angular frequency. In equations (10) and

(11) $\mathbf{Y}_S$ and $\mathbf{Y}_L$ are the input admittance matrices and $\mathbf{I}_S$ and $\mathbf{I}_L$ are vectors of current sources of a $n+1$-port Norton equivalent circuit as described in [23].

In this paper the parameter matrices $\mathbf{Z}$ and $\mathbf{Y}$ for each of the cables were experimentally identified from input impedances measurements taking into account their frequency-dependency, as described in [12, 24].

The resonance surface responses obtained from this model are described in the following sections, section 3 with a three-dimensional example and section 4 with a higher-dimensional surface.

3. Three-dimensional resonance surface response

In this section a three-dimensional resonance surface response example will be presented. For the surface to be 3D the analysis must be limited to two variables, the third dimension being used to present the results. This limitation forces two simplifications of the generic system in Fig. 2: the cable must have only two conductors, and one of the impedances Z_S or Z_L must be neglected. In this example, Z_S and I_L were canceled as shown in Fig. 3.

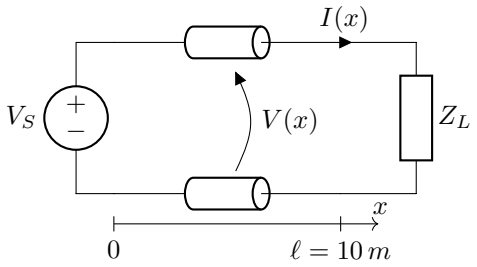

Figure 3: Schematics of the two-conductor cable system under study, the resonance analysis is performed in function of Z_L

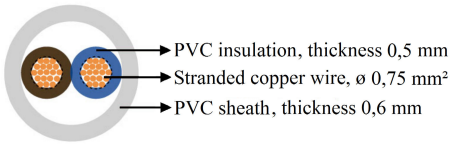

Figure 4: Cross-section of the two-conductor $0.75\,mm^2$ cable

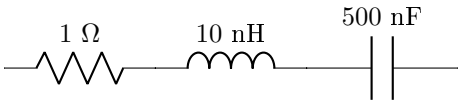

Figure 5: Z_{L_e}: Load chosen as example for the intersection with the resonance surface response

The current source in the general model was converted to a voltage source V_S for convenience, and the resonance surface response is plotted in function of the voltage $V(x)$.

The cable parameters come from two-conductor cable of section $0.75\,\mathrm{mm}^2$ commonly used in residential electrical plug extensions, its cross-section is presented in Fig. 4. They were identified from input impedance measurements and can be found in Fig. 2.30 of [24].

The resonance surface response is calculated by evaluating the voltage envelope along the 10 m long cable for all the combinations of the variables in table 1. The maximal voltage obtained for each pair (A, B) is then stored, along with the frequency and position where it takes place. In this section the voltage source is set to $V_S = 1$ V.

Table 1: Range of values used in the numerical analysis leading to the resonance surface response

Variable	Range	Number of points	Scaling
A	$[10^{-2}, 10^{5}]\ \Omega$	402	log
B	$[-10^{5}, -10^{-2}] \cup [10^{-2}, 10^{5}]\ \Omega$	402	log
f	$[0.1, 10]$ MHz	5000	log
x	$[0, 10]$ m	21	linear

To exemplify a possible reading from the resonance surface response the example load given in Fig. 5 is used.

The surfaces composing the resonance surface response are plotted in Fig. 6. In Figs. 6a and 6b are the maximal voltages obtained for each impedance

$Z_L = A + jB$, in Figs. 6c and 6d are the correspondent resonance frequencies and in Figs. 6e and 6f the position where the maximal voltage takes place. The figures are split in two to represent positive and negative values of B in log scale.

Note that the frequency and voltage amplification surfaces are mirrored: the higher is the voltage amplification the lower is the resonance frequency corresponding to it, because the cable losses are smaller for lower frequencies.

The resonance surface response presents three zones corresponding to the well-known behavior of the resonance phenomenon (propagation speed in the cable $v \approx 1.54 \times 10^8\, m/s$):

- The zone of high values of A or B: approaches the open-ended cable, resonance frequency of $f_r = v/4\ell$ taking place at $x = \ell$ with high voltage amplification;
- The zone of low values of A and B: approaches the short-circuited cable, resonance frequency of $f_r = v/2\ell$ taking place at $x = \ell/2$ with a voltage amplification lower than in the previous case;
- The zone of matched impedances $A \approx |Z_c|$ and $|B| < |Z_c|$ where resonance does not take place: the maximal voltage equals the input voltage $1V$ and there are discontinuities in the frequency and position surfaces.

The portion of the surface under the condition $|B| < |Zc|$ confirms the behavior described in [14]:

- for $|Z_L| < |Z_c|$ the resonance frequency is the same as for a short-circuited line
- for $|Z_L| > |Z_c|$ the resonance frequency is the same as for an open-ended line

However, the resonance frequency response shows that for loads with higher reactive components ($|B| > |Zc|$) this rule no longer applies. This is one of the

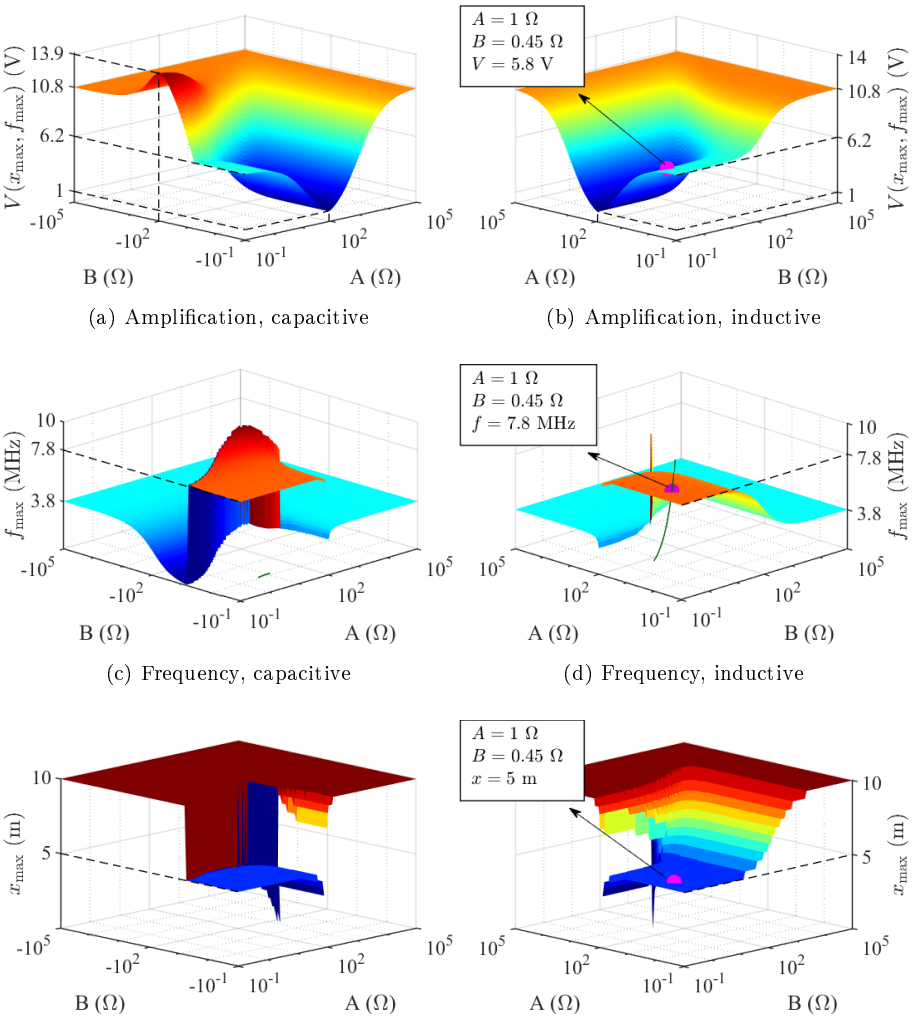

(a) Amplification, capacitive

(b) Amplification, inductive

(c) Frequency, capacitive

(d) Frequency, inductive

(e) Position, capacitive

(f) Position, inductive

Figure 6: Resonance Surface Response for $0,75mm^2$ two-conductor cable of length $\ell = 10\,m$; Line in green: impedance Z_{L_e}, markers in pink: intersections with Z_{L_e}

Table 2: Resonance behavior of the cable when connected to the example load Z_{L_e}

Resonance frequency f_r	7.8 MHz
Voltage amplification $V(x_r)/V(0)$	5.8
Position of maximal voltage x_r	5 m

main contribution of these surfaces: the resonance behavior of a cable can be assessed for any Z_L connected to the cable.

In this merit, two distinct behaviors of the resonance were exposed by the surface:

- The maximum voltage occurs for a capacitive load to which the resonance frequency is lower than in the open-ended cable.
- The zone corresponding to inductive loads presents the only resonance taking place not at the midpoint nor at the endpoint of the line, but varying in the interval $\ell_c/2 < x < \ell$.

To exemplify a reading from these surfaces, the impedance of the example load Z_{L_e} presented in Fig. 5 was plotted in green in function of the frequency in Figs. 6c and 6d. The intersection between Z_{L_e} and the frequency surface gives the resonance frequency of the cable terminated by Z_{L_e}. The resonance voltage and position can then be assessed with the respective points in the remaining surfaces, points marked in pink in Fig. 6. The resonance behavior of this example is resumed in table 2.

Two unprecedented analysis are proposed below to extend the applicability of the resonance surface response. They use 2D cuts from the 3D surface, in section 3.1 to compare the resonance behavior of different two-conductor cables and in section 3.2 to analyze the impact of cable length in the resonance behavior.

3.1. Comparing cables with cuts from the resonance surface response

This section proposes a method to compare the resonance behavior of different cables. One examples of applicability of this method is the cable selection

Table 3: Description of the cables to be compared for their resonance behavior; R and G given for $f = 1$ MHz, $|Z_c|$ its mean value in the band $f \in [1, 10]$ MHz

Cable	Application	$\lvert Z_c \rvert$ (Ω)	R ($\frac{\text{m}\Omega}{\text{m}}$)	G ($\frac{\mu S}{\text{m}}$)
Constant parameters	Example, $L = 578\text{nH/m}$ $C = 76,3$ pF/m	87	597.3	118.2
Two-conductor 0.75 mm^2	Residential plug extension	87.5	293.5	40.10
Two-conductor 1.5 mm^2	Audio cable	105	347.0	12.43
Two-conductor 2.5 mm^2	Power cord cable	71.8	251.9	25.19
Coaxial 50 Ω	RF signals	52.8	157.3	0.7610

in the design phase of a system vulnerable to conducted emissions.

Plotting several 3D surfaces in the same axis can make the data difficult to read, and for this reason sensible 2D cuts from the surfaces were selected for an easy visual comparison. The chosen cuts correspond to the intersection between the surfaces and the planes $B = 0$, $A = 0$ and $A = |Z_c|$.

The cables to be compared are described in table 3. The parameters of these cables were obtained with input impedance measurements, the parameters of the non-shielded cables and can be found in [24] and the parameters of the coaxial cable are plotted in the Appendix. A constant parameter example was added to show the implications of neglecting their frequency dependency to simplify the model.

In this analysis the computation time can be drastically reduced by calculating the surface points exclusively for the values of (A, B) present in the 2D cuts, what was done for the cables first included in this section. The cuts from the frequency and position surfaces could also be obtained, but here they are omitted for the sake of brevity.

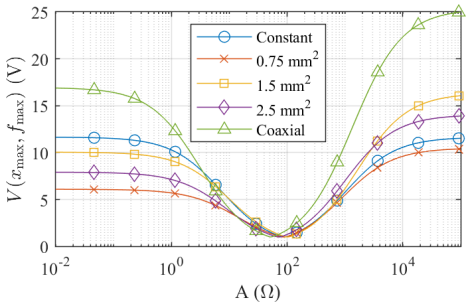

(a) $B = 0$, pure ressistive load

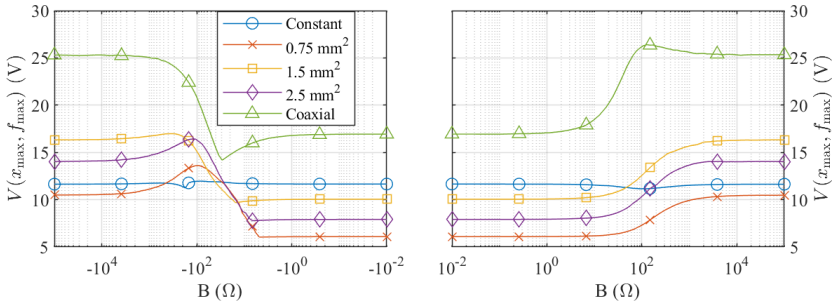

(b) $A = 0$, pure capacitive to the left, pure inductive to the right

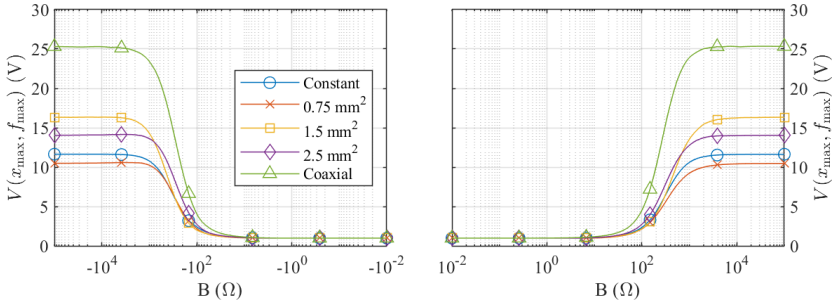

(c) $A = |Z_c|$, capacitive to the left, inductive to the right

Figure 7: Cuts from the resonance surface responses of the cables described in table 3

The 2D cuts of the voltage surface are plotted in Fig. 7. The first cut in Fig. 7a corresponds to $B = 0$ and shows the resonance voltage when the cable is connected to a pure resistive load. From it can be read the band around $|Z_c|$ where the behavior is close to impedance matching $Z_L = Z_c$, also can be compared the open-circuit (OC) and short-circuit (SC) resonance voltages. The cable with constant parameters has the same amplification for both OC and SC, as expected.

The second 2D cut $A = 0$ is plotted in Fig. 7b, and show the behavior of the resonance when the cable is connected to pure reactive loads. The peak of maximum voltage amplification is in the capacitive zone except for the coaxial cable that has its maximum voltage for an inductive load. These distinctions are not visible with the simplified model of constant p.u.l. parameters.

The last cut corresponds to $A = |Z_c|$ and is plotted in Fig. 7c. In this figure can be read the limit value of B that still allows the line to behave as a matched impedance line, in all cases this limit is around $B < |Z_c|$.

These 2D cuts from the resonance surface response are those that best represent the overall shape of the 3D surfaces and are en effective way to compare the resonance behavior of different cables.

3.2. Impact of cable length on the resonance surface response

At first, the impact of the cable length on voltage amplification due to resonance may not be evident. Indeed, the voltage amplification depends directly on the total losses in the cable given by the expression $\mathbb{R}\{\gamma\ell\} = \alpha\ell$, were α is the attenuation coefficient, a direct representation of the cable losses.

The parameter α increases with frequency. The relevant value of α impacting the voltage amplification is $\alpha(f_r)$, with f_r the resonance frequency. Two characteristics must be considered:

- A longer cable will have higher total losses $\alpha\ell$ given a constant α, however;
- A longer cable will have a lower f_r, and therefore a lower $\alpha(f_r)$.

To study this aspect, an analysis specific to the voltage at $x = \ell$ of an open-ended cable was done. The resonance frequency of an open-ended cable is given by (12), what allows the approximation of $Z(0)$ for an open-ended cable at the resonance frequency f_r given in (13) [13]. The equation giving $V(\ell)$ is recalled in (14), what gives $V(\ell)^{OC}$ for $f = f_r$ as in (15).

$$f_r = \frac{v}{4\ell} \tag{12}$$

$$Z^{OC} \overset{f=f_r}{=} Z_c \coth(\alpha\ell) \approx Z_c \alpha\ell \tag{13}$$

$$V(\ell) = V(0)\left[\cosh(\gamma\ell) + \frac{Z_c}{Z^{OC}}\sinh(\gamma\ell)\right] \tag{14}$$

$$V(\ell)^{OC} \overset{f=f_r}{=} \frac{V_s}{\alpha\ell} \tag{15}$$

The applicability of this approximation is demonstrated in Fig. 8. In this figure, a numerical solution using the frequency-domain model described in section 2, following the principles of the resonance surface response, extracted the highest $V(\ell)$ from different excitation frequencies for the $2,5$ mm^2 cable with length varying form 4 m to 50 m. This numerical solution is then compared to the same voltage calculated from equation (15), first using the attenuation coefficient corresponding to the resonance frequency f_r given by (12) and secondly using α for $9.8\,MHz$, the resonance frequency of a 4 m long cable.

Fig. 8 shows that the factor $\ell\,\alpha(f_r)$ increases with the cable length despite the reduction of the resonance frequency, attenuating the resonance voltage. Still, this attenuation would be greater if the cable losses were constant (dashed line).

To generalize this analysis, the resonance surface response is again necessary. They were calculated for three different lengths of the $2,5$ mm^2 cable and for most of the regions of the surface the voltage amplification was reduced by a constant factor as length increases except for pure reactive loads.

For this reason the cut $A = 0$ is the only to be presented here in Fig. 8. It shows that, other than the fact that the voltage amplification reduces with cable length, the resonance voltage peak for capacitive loads around $B = -10^2\ \Omega$ is

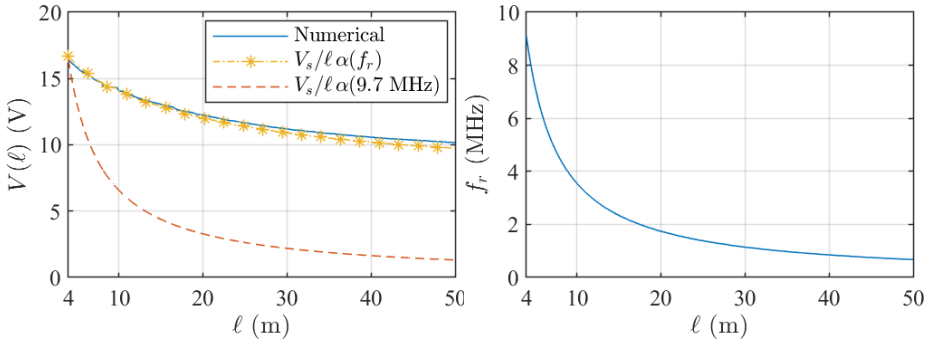

(a) $V(\ell)$ under resonance (b) f_r of the open-ended cable

Figure 8: Analysis of the open-ended 2.5 mm^2 cable. In (a) $V(\ell)$ in function of cable length ℓ, the numerical solution (full line) is compared to (15) with both $\alpha(f_r)$ in asterisks and $\alpha(9.8\text{ MHz})$ in the dashed line; the resonance frequency f_r is given in (b), and 9.8 MHz corresponds to f_r for $\ell = 4$ m

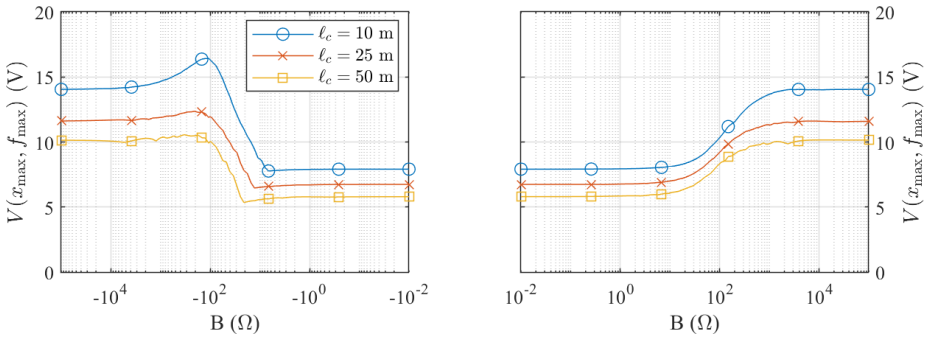

Figure 9: Cut $A = 0$ of the resonance surface response of the 2.5 mm^2 cable for different cable lengths

attenuated as the cable length increases.

In conclusion, longer power cables tend to have lower harmonic amplifications, even if their attenuation may be lesser than expected.

4. Higher-dimensional resonance surface response

The three-dimension resonance surface response presented in the previous section applies exclusively to systems with two-conductor cables. If the circu-

lation of parasitic currents is considered it is likely that a system will not be accurately represented by the two-conductor cable model.

Therefore, to expand the applicability of these surfaces the multiconductor TL model must be studied, what demands the analysis of the resonance surface response of higher dimensions. This is one of the key novelties of this paper.

A generic model of a system with a $(n+1)$-conductor cable would have the terminals connected to $(n+1)$-port Thévénin/Norton equivalent circuits, as shown in Fig. 2. For these equivalent circuits to be generic, they would require at least $(n+1)n/2$ impedances to be identified [23]. As the resonance surface response needs an axis to represent each the real and the imaginary part of the impedances composing $\mathbf{Z_S}$ and $\mathbf{Z_L}$, plus one axis to represent the result variable (maximal voltage/current, frequency, position) the resonance surface response has $2(n+1)n+1$ dimensions for a $(n+1)$-conductor cable in its most generic representation.

If the impedance matrix $\mathbf{Z_S}$ and source vector $\mathbf{I_L}$ are canceled reducing the system to a simple source-line-load schematic, still $(n+1)n+1$ dimensions are needed for a $(n+1)$-conductor cable, and the surface cannot be visualized for $n > 1$.

The decomposition of a system with a $(n+1)$-conductor cable into n modal two-conductor systems is possible according to the theory described in [25, 26]. The decomposition proposed is these works is based on the diagonalization of p.u.l. parameter matrices $\mathbf{YZ}$ and $\mathbf{ZY}$ with a decomposition matrix $\mathbf{T}$.

However, in power cables these parameters vary considerably with frequency, and in the general case different $\mathbf{T}$ are needed for different frequencies. A 3D resonance surface response derived from a frequency-dependent decomposition would have no meaning at all: modal voltages on different basis cannot be compared.

Moreover, for the whole system to be decomposed $\mathbf{T}$ should also diagonalize $\mathbf{Z_L}$, what is not guaranteed in the most general case.

That leaves two options of analysis, depending on the system characteristics:

- A single frequency independent transformation allows the decomposition of the $n+1$-conductors cable model, the source and load equivalent circuits into n two-conductor modal subsystems, and the resonance frequency response can be plotted in 3D for each mode.

- Such a transformation is not possible, and the resonance frequency response will be in higher dimensions. Even though it cannot be plotted, an optimization algorithm can be used analyze it.

These two possibilities are studied in the next two subsections, respectively.

4.1. Frequency independent decomposition of systems with multiconductor cables

As aforementioned, to represent systems with multiconductor cables with 3D resonance surfaces a single frequency independent $\mathbf{T}$ able to diagonalize all the matrices modeling the system ($\mathbf{YZ}$, $\mathbf{ZY}$, $\mathbf{Z_L}$ and $\mathbf{Z_S}$, cf. Fig. 2) is needed. There are special cases where this is possible.

A first example is a three-conductor balanced system, i.e. a system with decoupled common mode (CM) and differential mode (DM), assuming that the third conductor is the common-mode path, e.g. cable shield or earth return. The CM/DM decomposition is given by equations (16) and (17).

$$V_{DM} = V_1 - V_2 \qquad I_{DM} = \frac{I_1 - I_2}{2} \tag{16}$$

$$V_{CM} = \frac{V_1 + V_2}{2} \qquad I_{CM} = I_1 + I_2 \tag{17}$$

For the system to be balanced, all elements source, cable and load must be balanced [27]. For a cable to be balanced it has to be cyclic symmetric [**?**], i.e. the cross-section of the cable has the same geometry if it is rotated of a symmetry angle θ.

These observations lead to the generalization of this example: a frequency independent modal decomposition of a $n+1$-conductor system is possible if the cable, the load and the source are cyclic symmetric. If that is the case, the parameters matrices $\mathbf{Z}$ and $\mathbf{Y}$ and terminal matrices $\mathbf{Z_L}$ and $\mathbf{Z_S}$ are circulant

[?], and a possible orthonormal decoupling matrix $\mathbf{T}$ is given by (18) (see [22] on page 300 for more details)

$$[\mathbf{T}]_{ij} = \frac{1}{\sqrt{n}} \exp[\frac{2\pi}{n}(i-1)(j-1)] \tag{18}$$

It is true that many power cables are cyclic symmetric, but cyclic symmetric devices (loads) with $n > 2$ are less common. One rare example is three-phase electrical motors.

An example of 3D resonance surface response for a three-conductor balanced system using the differential/common-mode decomposition can be found in a previous work by the same authors [21]. The systems that do not present cyclic symmetry can only be analyzed by the general approach described in the next section.

4.2. seven-dimensional surface

Higher dimensional surfaces are needed to describe a system with multi-conductor cables. Here the resonance surface response of a three-conductor cable will be studied, taking the hypothesis that all currents circulate exclusively through these three conductors (no earth return).

In this example, the generic schematic from Fig. 2 was simplified by canceling $\mathbf{Z_S}$ and $\mathbf{I_L}$, and transforming the current sources $\mathbf{I_S}$ into voltage sources, for convenience. The resonance surface response will be computed in function of the maximum between $V_1(x)$ and $V_2(x)$.

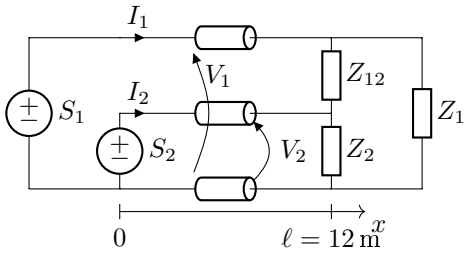

Figure 10: Schematics of a generic model for a three-conductor cable system, the resonance analysis is performed in function of the load impedances Z_1, Z_{12}, Z_2

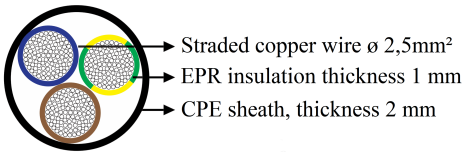

Figure 11: $2.5\,\mathrm{mm}^2$ three-conductor cable cross-section

The resonance surface response of the cable in Fig. 10 requires one axis for each the real and imaginary parts of each of the three load impedances plus one axis for the results of the resonance voltage, frequency or position. Therefore, seven dimensions are needed to describe the surface (as stated above: $(n+1)n+1$ with $n = 2$).

This surface cannot be plotted, but an optimization algorithm will be used to investigate it. Thus, the surface is not entirely calculated, instead the optimization algorithm chooses the points to be evaluated on its search for a maximum in the voltage surface.

For this example the parameters from a three-conductor cable of section $2.5\,\mathrm{mm}^2$ are used, this cable was designed for power cords of single-phase devices needing a protective earth (PE) conductor. A cross-section of the cable is presented in Fig. 11. The parameters of the cable were obtained with an identification based on input impedance measurements and can be found in Fig. 3.19 of [24].

The amplitude of the sources feeding the cable are fixed at $S_1 = 1.5$ V and $S_2 = 0.5$ V, so that the equivalent sources in differential and common mode have both an amplitude of 1 V (see equations (16) and (17)).

The goal function for this problem is to minimize the function (19) that has its minima corresponding to the maxima between the two voltages $V_1(x, f)$ and $V_2(x, f)$, and in which the regions around the minima are dilated by the exp function.

$$F(X) = -\exp[\max[V_1(x, f), V_2(x, f)]] \tag{19}$$

In this study, an initial analysis was performed to investigate the general

Table 4: Scaling of variables and goal function domain of the resonance surface response optimization with the sequential quadratic programming (SQP) algorithm, with soft constraints.

Variable	Scale	Range
f	linear	$[1, 10]$ MHz
x	linear	$[0, \ell_c]$ m
A_1, A_{12}, A_2	log	$[0] \cup [10^{-2}, 10^{6}]\,\Omega$
B_1, B_{12}, B_2	log	$[-10^{6}, -10^{-2}] \cup [0] \cup [10^{-2}, 10^{6}]\,\Omega$

behavior of the surface identifying multiple local maxima for different load impedances; it is described in subsection 4.2.1. To refine the results, a second analysis with additional constraints based on a real system was performed, resulting in one single point of maximum voltage; this is described in 4.2.2.

4.2.1. Soft-constrained optimization

In the first stage of this analysis a loosely constrained optimization is performed with a deterministic algorithm, (sequential quadratic programming - SQP) in the domain described in table 4.

The optimization results on different maxima for different initial points, meaning that the surface has multiple local maxima. These points can give an intuition of how the surface behaves and for that reason a systematic method was established to obtain as many local maxima as possible.

The deterministic optimization was performed for 50 random initial points generated from a Sobol sequence that fills the space uniformly [28]. Six different local maxima were identified with this method, and are represented with numeric rulers in Fig. 12.

It cannot be guaranteed that these are all the local maxima, but they are enough to show that a very similar voltage amplification can be obtained with a different combination of impedance loads.

However, in a practical application the optimization constraints would be stronger and it is possible that a unique solution is found. This is discussed in

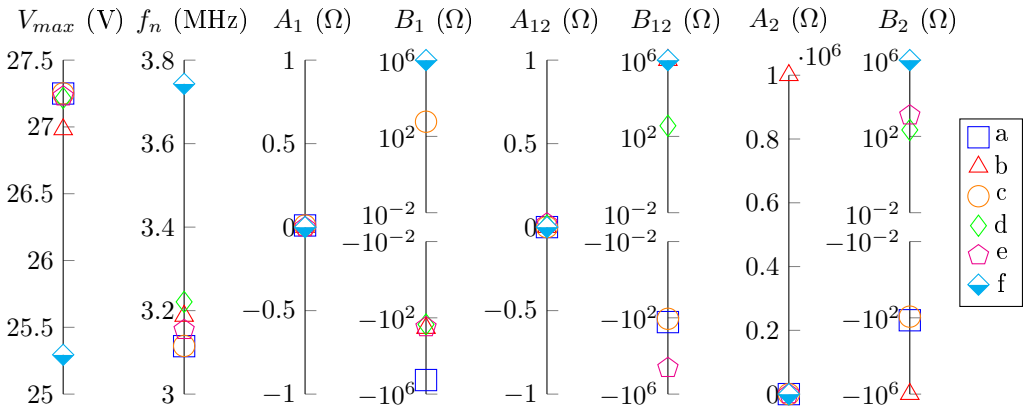

Figure 12: Light-constrained optimization results, six local maxima plotted in the 8 numeric rulers; all maxima occurred for $x = \ell$

the next subsection.

4.2.2. Strongly constrained optimization

In the second stage of this study, the constraints of the optimization problem were modified to adapt to a more realistic scenario, as follows: conductor 2 is the phase conductor, conductor 1 is the neutral conductor and conductor 0 is the protective earth (PE). The PE conductor is connected to the chassis of devices to ensure the user safety against electrical faults.

In this scenario the impedances Z_1 and Z_2 represent parasitic capacitances between the circuitry and the chassis, i.e. common-mode capacitances, and Z_{12} represents the device input impedance, i.e. the differential-mode impedance.

The assigned roles of each impedance allow the inclusion of new constraints in the optimization. We take the hypothesis that differential-mode input impedance will not assume higher values than 1 kΩ, and that the common-mode capacitances will not be greater than 100 pF, what gives the constraints in table 5.

The constrained optimization was performed with a genetic algorithm (GA) coupled with a deterministic algorithm (SQP). With the parameters given in 5, the optimization finds a single voltage maximum systematically, given in table 6.

Table 5: Extra constraints for the second stage of the study, optimization run with genetic algorithm (GA) followed by a sequential quadratic programming (SQP) algorithm.

Diff. mode	$\lvert Z_{12}\rvert < 1\,\mathrm{k\Omega}$
Common mode	$Z_1,\, Z_2 = -jB, \quad B \in \left[\dfrac{1}{2\pi f 100\,\mathrm{pF}}, 1\,\mathrm{M\Omega}\right]$

Table 6: Comparison of the constrained optimization result with the closest local maxima from Fig. 12

	Constrained optimization	Point "a" of Fig. 12
V_{max}	27.12 V	27.25 V
f_{max}	3.27 MHz	3.11 MHz
Z_1	$-j487.4\ \Omega$	$-j183.3\ \mathrm{k\Omega}$
Z_{12}	$-j1\ \mathrm{k\Omega}$	$-j167.5\ \Omega$
Z_2	$-j1.381\ \mathrm{k\Omega}$	$-j134.0\ \Omega$

The characteristics of point "a" from Fig. 12 are also listed in table 6 for comparison. It is the closest point to the optimum from the previous analysis, even if point "a" wold be outside de domain of the constrained problem (cf. table 5).

The resonance configuration given in 6 can be reproduced by the load in Fig. 13a. The simulation of the voltages of the cable connected to this load in function of the frequency are plotted in Fig. 13b. This plot shows the possible amplification of parasitic harmonics if their frequency is close to the resonance.

Fig. 13b

It is unlikely that a real single-phase device would have the input impedance given in Fig. 13a, what is an indicator that the chosen constraints in table 5 are still more loose than desired. However, in a real case application these constraints could be more easily defined and the results would be more realistic. It is strongly recommended that, if the maximum voltage in a real system is to

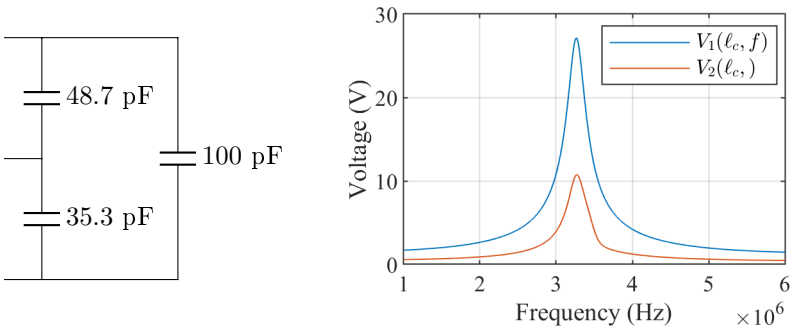

(a) (b)

Figure 13: (a): equivalent load of the maximum voltage amplification point in table 6 and (b): corresponding simulation of the voltages at $x = \ell_c$.

be calculated, the optimization constraints are defined is finely as possible.

Note that the critical load in Fig. 13a is not balanced, therefore could not be found with an analysis based on a common, differential-mode decomposition as discussed in section 4.1 and detailed in [21]. Only the analysis of higher dimension surfaces proposed here is able to characterize the resonance behavior of a generic system.

5. Conclusion

The resonance surface response can be a very useful tool in the design of systems robust against switched harmonics circulating in long portions of cable. It requires a complete model of the system, what makes this approach more useful in applications such as the design of electric vehicles or electric power plants, where the whole system is known to the developers. The resonance surface response can come to the aid of the designers by ensuring an accurate prediction of the conducted emission amplitude, thus guaranteeing a sufficient robustness for the input filter of the electronic devices, the cable insulation, etc... The higher-dimensional surfaces, coupled with a well adapted optimization algorithm, allows the representation of any linear, or linearized, system in function of any number of variables. In this paper the components of the elec-

trical impedance were used as variables, but the surfaces can also be plotted in function of the physical elements of filter, for example. Therefore, in real-world applications the method for exploring the resonance surface response with an optimization algorithm proposed here should be adapted to the designer's needs.

References

[1] M. Cirrincione, M. Pucci, G. Vitale, Direct power control of three-phase VSIs for the minimization of common-mode emissions in distributed generation systems, Electric Power Systems Research 81 (4) (2011) 830–839. doi:10.1016/j.epsr.2010.11.007.
URL http://www.sciencedirect.com/science/article/pii/S0378779610002798

[2] Marios C. Sousounis,, Jonathan K. H. Shek,, Markus A. Mueller, Filter Design for Cable Overvoltage and Power Loss Minimization in a Tidal Energy System With Onshore Converters, IEEE TRANSACTIONS ON SUSTAINABLE ENERGY 7 (1) 400 – 408.

[3] S. Zhang, S. Jiang, X. Lu, B. Ge, F. Z. Peng, Resonance Issues and Damping Techniques for Grid-Connected Inverters With Long Transmission Cable, IEEE Transactions on Power Electronics 29 (1) (2014) 110–120. doi:10.1109/TPEL.2013.2253127.

[4] S. Liu, F. Lin, X. Fang, Z. Yang, Z. Zhang, Train Impedance Reshaping Method for Suppressing Harmonic Resonance Caused by Various Harmonic Sources in Trains-Network Systems With Auxiliary Converter of Electrical Locomotive, IEEE Access 7 (2019) 179552–179563. doi:10.1109/ACCESS.2019.2958880.

[5] L. Zhai, X. Zhang, N. Bondarenko, D. Loken, T. P. Van Doren, D. G. Beetner, Mitigation Emission Strategy Based on Resonances from a Power Inverter System in Electric Vehicles, Energies 9 (6) (2016) 419. doi:10.

3390/en9060419.
URL https://www.mdpi.com/1996-1073/9/6/419

[6] D. Drozhzhin, G. Griepentrog, A. Sauer, R. D. Maglie, A. Engler, Investigation on differential to common mode coupling in the output cable of AC drive for more electric aircraft, in: 2017 19th European Conference on Power Electronics and Applications (EPE'17 ECCE Europe), 2017, pp. P.1–P.9. doi:10.23919/EPE17ECCEEurope.2017.8098927.

[7] R. J. Kerkman, D. Leggate, G. L. Skibinski, Interaction of drive modulation and cable parameters on AC motor transients, IEEE Transactions on Industry Applications 33 (3) (1997) 722–731. doi:10.1109/28.585863.

[8] H. Akagi, I. Matsumura, Overvoltage Mitigation of Inverter-Driven Motors With Long Cables of Different Lengths, IEEE Transactions on Industry Applications 47 (4) (2011) 1741–1748. doi:10.1109/TIA.2011.2154294.
URL http://ieeexplore.ieee.org/document/5766034/

[9] H. D. Paula, D. A. d. Andrade, M. L. R. Chaves, J. L. Domingos, M. A. A. d. Freitas, Methodology for Cable Modeling and Simulation for High-Frequency Phenomena Studies in PWM Motor Drives, IEEE Transactions on Power Electronics 23 (2) (2008) 744–752. doi:10.1109/TPEL.2007.915759.

[10] L. Wang, C. N.-M. Ho, F. Canales, J. Jatskevich, High-Frequency Modeling of the Long-Cable-Fed Induction Motor Drive System Using TLM Approach for Predicting Overvoltage Transients, IEEE Transactions on Power Electronics 25 (10) (2010) 2653–2664. doi:10.1109/TPEL.2010.2047027.

[11] D. d. P. d. Santos, C. A. F. Sartori, Impact of mismatch cables impedances on active motor terminal overvoltage mitigation using parallel voltage source inverters, in: 2017 IEEE 3rd Global Electromagnetic Compatibility Conference (GEMCCON), 2017, pp. 1–6. doi:10.1109/GEMCCON.2017.8400662.

[12] T. G. Bade, J. Roudet, J.-M. Guichon, et. al., Frequency-domain modeling of unshielded multiconductor power cables for periodic excitation with new experimental protocol for wide band parameter identification, Electrical Engineering (2019) 1–11.

[13] W. C. Johnson, Transmission lines and networks, McGraw-Hill, 1950.

[14] A. I. Chrysochos, T. A. Papadopoulos, G. K. Papagiannis, Rigorous calculation method for resonance frequencies in transmission line responses, IET Gener., Transm. & Distrib. (nov 2014).

[15] A. Pană, A. Băloi, F. Molnar-Matei, A Numerical Analysis of the Harmonic Impedance in a Medium Voltage AC Network, in: 2019 8th International Conference on Modern Power Systems (MPS), 2019, pp. 1–6.

[16] D. Darmawardana, S. Perera, J. Meyer, D. Robinson, U. Jayatunga, S. Elphick, Development of high frequency (Supraharmonic) models of small-scale (<5kw), single-phase, grid-tied PV inverters based on laboratory experiments, Electric Power Systems Research 177 (2019) 105990. doi:10.1016/j.epsr.2019.105990.
URL http://www.sciencedirect.com/science/article/pii/S0378779619303098

[17] B. Revol, J. Roudet, J. Schanen, et al., Emi study of three-phase inverter-fed motor drives, IEEE Trans. on Ind. App. (jan/feb 2011).

[18] Z. Chen, A. Luo, H. Kuang, L. Zhou, Y. Chen, Y. Huang, Harmonic resonance characteristics of large-scale distributed power plant in wideband frequency domain, Electric Power Systems Research 143 (2017) 53–65. doi:10.1016/j.epsr.2016.09.001.
URL http://www.sciencedirect.com/science/article/pii/S0378779616303509

[19] C. F. Jensen, Harmonic background amplification in long asymmetrical high voltage cable systems, Electric Power Systems Research 160 (2018)

292–299. doi:10.1016/j.epsr.2018.03.009.
URL http://www.sciencedirect.com/science/article/pii/S0378779618300816

[20] I. Sowa, J. L. Domínguez-García, O. Gomis-Bellmunt, Impedance-based analysis of harmonic resonances in HVDC connected offshore wind power plants, Electric Power Systems Research 166 (2019) 61–72. doi:10.1016/j.epsr.2018.10.003.
URL http://www.sciencedirect.com/science/article/pii/S0378779618303201

[21] T. G. Bade, J. Roudet, J.-M. Guichon, et. al., Robust filter design technique to limit resonance in long cables connected to power converters, IEEE Trans. on EMC (2020). doi:10.1109/TEMC.2020.2993082.

[22] C. Paul, Analysis of multiconductor transmission lines, IEEE Press, 2008.

[23] M. Hosoya, The simplest equivalent circuit of a multi-terminal network, Bull. Fac. Sci., Univ. Ryukyus, 70 (2000) 1–10.

[24] Bade, T. G. , Characterization of the Cabling on Industrial Power Networks for EMI Simulation, Phd thesis, Communauté UGA (2019).
URL https://hal.archives-ouvertes.fr/tel-02409933

[25] G. G. Gentili, M. Salazar-Palma, The definition and computation of modal characteristic impedance in quasi-tem coupled transmissionlines, IEEE Trans. on Microw. Theory and Tech. (1995) 338 – 343.

[26] C. R. Paul, Decoupling the multiconductor transmission line equations, IEEE Trans. on Microw. Theory and Tech. 44 (1996) 1429 – 1440.

[27] A. Sugiura, Y. Kami, Generation and Propagation of Common-Mode Currents in a Balanced Two-Conductor Line, IEEE Trans. on EMC 54 (2) (Apr. 2012). doi:10.1109/TEMC.2011.2162523.

[28] S. Joe, F. Y. Kuo, Remark on algorithm 659: Implementing sobol's quasirandom sequence generator, ACM Transactions on Mathematical Software (TOMS) 29 (1) (2003) 49–57.

Appendix

The parameters of the coaxial cable obtained with an identification based on the input impedance measurement [12] are plotted in Fig. 14.

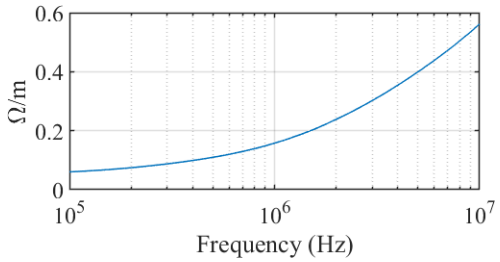

(a) Resistance

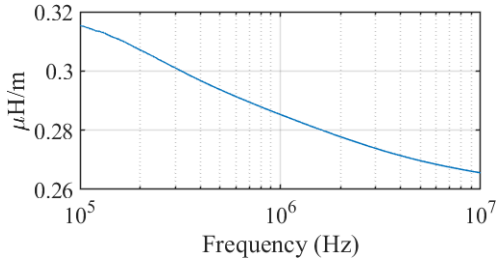

(b) Inductance

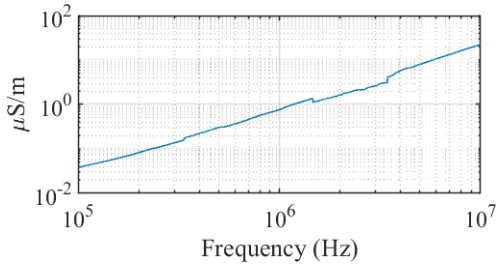

(c) Conductance

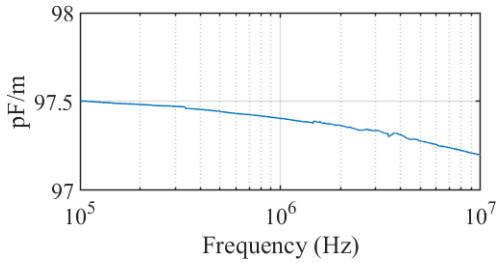

(d) Capacitance

Figure 14: Per-unit-length parameters of the coaxial cable introduced in section 3